AD_____


Award Number:  W81XWH-�Ì ËÏÍ G


TITLE: Ú[¦¸æà|^ÁV|dæ[ˇ}åÁQ æ‡ã¸*Á–Ás@¸ÁÓ¦æã¸ÁÁ[¦Á•^¸Ás¸ÁÐ[¸¸æàåÁÒææd^-ã¦|åÁOE^æ•


PRINCIPAL INVESTIGATOR: Õ¦^*[¦^ÁÔ|^{ ^}c


CONTRACTING ORGANIZATION: U|dæÁÖã懸}[•æã•¸ÊÁQ¸&È
                    Þ[¦¸o@ÁÓæd^-à[¦[ ¸ÊÁT OÁÆ€Gï Î€Á


REPORT DATE:  T¸æ&@ÁG€FF


TYPE OF REPORT:  Annual


PREPARED FOR:  U.S. Army Medical Research and Materiel Command
            Fort Detrick, Maryland  21702-5012


DISTRIBUTION STATEMENT:  Approved for public release; distribution unlimited

# REPORT DOCUMENTATION PAGE

Public reporting burden for this collection of information is estimated to average 1 hour per response, including the time for reviewing instructions, searching existing data sources, gathering and maintaining the data needed, and completing and reviewing this collection of information. Send comments regarding this burden estimate or any other aspect of this collection of information, including suggestions for reducing this burden to Department of Defense, Washington Headquarters Services, Directorate for Information Operations and Reports (0704-0188), 1215 Jefferson Davis Highway, Suite 1204, Arlington, VA 22202-4302. Respondents should be aware that notwithstanding any other provision of law, no person shall be subject to any penalty for failing to comply with a collection of information if it does not display a currently valid OMB control number. **PLEASE DO NOT RETURN YOUR FORM TO THE ABOVE ADDRESS.**

| 1. REPORT DATE *(DD-MM-YYYY)* | 2. REPORT TYPE | 3. DATES COVERED *(From - To)* |
|---|---|---|
| 01-03-2011 | Annual | 31 MAR 2010-28 FEB 2011 |

| 4. TITLE AND SUBTITLE | 5a. CONTRACT NUMBER |
|---|---|
| Portable Ultrasound Imaging of the Brain for Use in Forward Battlefield Areas | |
| | 5b. GRANT NUMBER |
| | W81XWH-08-1-0152 |
| | 5c. PROGRAM ELEMENT NUMBER |

| 6. AUTHOR(S) | 5d. PROJECT NUMBER |
|---|---|
| Gregory Clement | |
| | 5e. TASK NUMBER |
| E-Mail: gclement@hms.harvard.edu | 5f. WORK UNIT NUMBER |

| 7. PERFORMING ORGANIZATION NAME(S) AND ADDRESS(ES) | 8. PERFORMING ORGANIZATION REPORT NUMBER |
|---|---|
| Ultra Diagnostics, Inc. North Attleboro, MA 02760 | |

| 9. SPONSORING / MONITORING AGENCY NAME(S) AND ADDRESS(ES) | 10. SPONSOR/MONITOR'S ACRONYM(S) |
|---|---|
| U.S. Army Medical Research and Materiel Command Fort Detrick, Maryland 21702-5012 | |
| | 11. SPONSOR/MONITOR'S REPORT NUMBER(S) |

**12. DISTRIBUTION / AVAILABILITY STATEMENT**

Approved for Public Release; Distribution Unlimited

**13. SUPPLEMENTARY NOTES**

**14. ABSTRACT**

Not provided.

**15. SUBJECT TERMS**

Not provided.

| 16. SECURITY CLASSIFICATION OF: | | | 17. LIMITATION OF ABSTRACT | 18. NUMBER OF PAGES | 19a. NAME OF RESPONSIBLE PERSON USAMRMC |
|---|---|---|---|---|---|
| a. REPORT U | b. ABSTRACT U | c. THIS PAGE U | UU | 17 | 19b. TELEPHONE NUMBER *(include area code)* |

# TABLE OF CONTENTS

# INTRODUCTION

The overall goal of this project has been to develop (i) an ultrasound-based detection system designed to detect foreign bodies in the brain and (ii) a portable ultrasound-based imaging system capable of producing full brain images through the intact skull.

This year, based on preliminary designs and testing in Years I and II of the project, a final design and reconstruction approach has been established. Key findings and considerations leading to the design have been:

- The determination that in many regions of the brain -particularly in critical areas in the center of the brain - access angles via shear-mode transcranial windowing through the skull bone simultaneously produce longitudinal modes that can interfere with the shear mode imaging.

- Signal-to-noise rations of the shear-mode-windowed signals can be greatly enhanced using narrow-band transmission signals.

- Image resolution at the reduced operating frequency necessary to achieve transcranial propagation greatly benefit from an extended degree of imaging angles.

These findings have resulted in improvements to transducer design, electronics, and imaging sequence. In the final system currently in construction, two rapid planning stages will correct both the incoming and outgoing waves, and a novel reconstruction algorithm will generate 2D image slices, including full cross-sections, thus providing anatomical orientation paralleling that of CT or MRI. We will accomplish this by combining several techniques developed over the past 12 months to both correct for distortion and maximize the energy transferred through the bone. The approach is based upon well-established diffraction tomography theory, but with a novel beamforming method that will maximize the reconstructed signal. Beam correction previously developed for noninvasive ultrasound therapy will also be utilized, but updated so that the correction is based solely on real-time ultrasound information, as opposed to past methods which required modeling using prior CT scans. It is expected that the locations of major echogenic intracranial anatomical structures (e.g. midline falx, mesencephalic brainstem, ventricle margins, etc.) can be accurately and precisely imaged, along with all abnormalities currently detectable with ultrasound only after craniotomy, or in pediatric cranial ultrasound (cUS) through the fontanelle.

In comparison with the initial transcranial probe developed in Year II, the transducer in construction will offer large angle viewing, allowing full tomographic reconstruction in order to produce clear and recognizable image features, and replacing the need to fuse US images with other modalities. Studies performed over the past year have validated the techniques necessary to perform the proposed imaging, and have simulated the planned fully-operating system through computer modeling and experimental mock-up.

Key components of the method include ultrasound measurement of skull thickness and sound speed, phase correction of beam distortion, the tomographic reconstruction algorithm, and the final image display. We have confirmed in preliminary studies that these techniques can be applied through the human skull. Now these components will be optimized as a function of transducer geometry, operation frequency, and number of elements via a combination of simulation and laboratory measurement, in order to determine the best possible design.

An ultrasound driving system is being customized to allow backscatter tomographic capability. Using transducer characteristics determined in a detailed simulation study this year, a ring-shaped probe is being constructed and combined with a standoff designed for straightforward patient coupling. Additional electronics based on modification of our existing imaging system are in the process of being assembled along with a computer-controlled operation interface and image display.

In the period of the one year no cost extension, the device and associated signal processing methodologies will be validated by registered comparison with magnetic resonance imaging (MRI). Utilizing human skull samples and a bank of ultrasound brain phantoms, identifiable structural features and abnormalities within both MRI and ultrasound modalities will be analyzed. Correlations between the two sets of data will be examined to quantify sensitivity, specificity, and repeatability. The ability to further enhance imaging by combining the approach with phase-corrected real-time b-mode, Doppler, and transmission imaging will also be examined.

This system is devised to expand the paradigm of US to include a new high-resolution and high SNR means for brain imaging, while maintaining the portability, safety, and cost advantages associated with ultrasound. Stationary image slices fused with phase-corrected Doppler using the same array will offer both anatomical views and flow assessment in the intracranial vessels.

The skull bone notwithstanding, the brain is one of the few organs that can be accessed from a wide range of viewing angles, opening the potential for full ultrasound computed tomography. Clinically implemented in breast tomography, UCT techniques have generally used a simplified linear back-projection, or a refracted-ray approach [1] in order to make real-time implementation practical [2] and to avoid uniqueness issues associated certain iterative methods. However, since ultrasound uses extremely large wavelengths compared x-ray or optical tomography, conventional tomographic theory is invalid for most situations.

Based on mockups performed this year, we expect that anatomy and abnormalities of the brain could be reconstructed, provided that ultrasound can both penetrate the skull and produce a coherent imaging source. We propose a corrective technique that will use ultrasound-based phased-array beam correction [3], optimized frequency selection [4], and a shear-mode windowing technique [5]. The approach is based upon the pioneering work of Smith and colleagues [6], [7], and is designed to overcome the major barriers to imaging through the skull in a manner that is robust and clinically feasible. A unique UCT reconstruction algorithm is
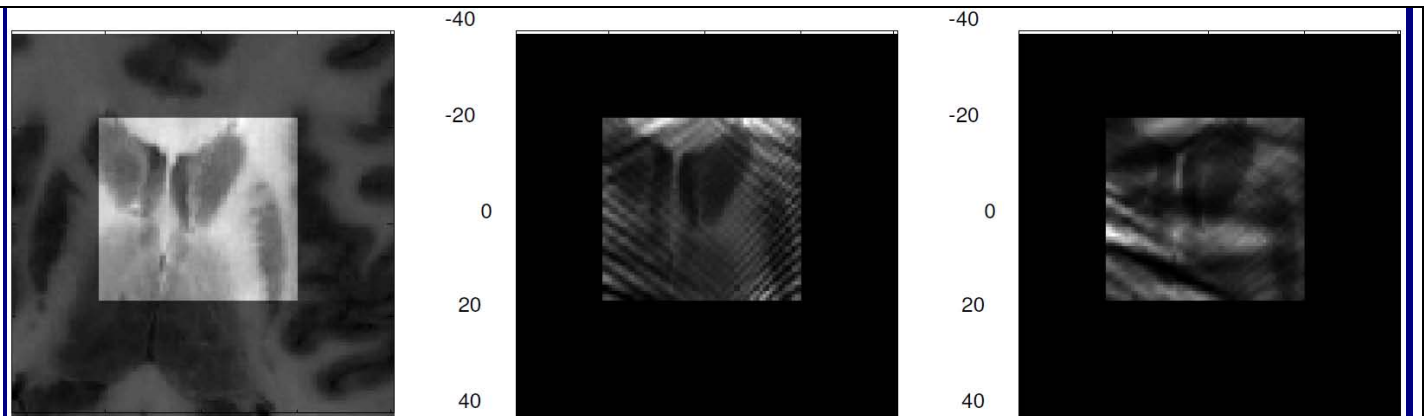


Fig 1. **Full mockup of the procedure** was performed with a numeric US phantom formed using segmented slices from the Human Body Project (image, left with ROI highlighted, scale in mm). This mockup included transcranial propagation and planning. The reconstructed ROI at 1.5 MHZ (center) is compared with the same image formed through the skull without correction (right). Segments of ROI reconstruction will be combined with skull outline measurement (Fig. 4) to provide a brain slice. The pase year has concentrated on optimizing the method performed here with somewhat arbitrary ultrasound parameters. One expected benefit of frequency mixing will be the elimination of "stripe" artifacts.

being implemented with the goal of producing images that are more detailed than conventional ultrasound, while also providing recognizable anatomical features to orient the operator (Fig 1). The device will use a backscatter tomographic technique, but also will be capable of immediately fusing these stationary images with b-mode ultrasound, Doppler, and transmission tomography [8] using the same array.

Successful implementation of the device and method could substantially aid the ability for early detection of such disorders as hematoma, tumors, swelling, hydrocephalus, vascular occlusion, and hemorrhage in the brain. The completed device will be approximately the size of a typical ultrasound imager. It is expected that the portability of the device will make its use practical in remote locations, the emergency room, operating room, patient bedside, and in an outpatient setting; all places where larger imaging devices are generally impractical due to size, maintenance, and cost.
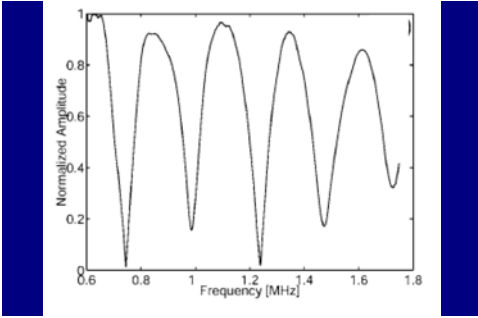
# BODY

## 1. Final Reconstruction method



Fig 2 Peaks in the transmission frequencies occur due to the skull's multi-layer transmission behavior. Natural variation causes the magnitude and spacing of the peaks to vary with position (hydrophone data through human skull bone, shown after normalization by peak transmission).
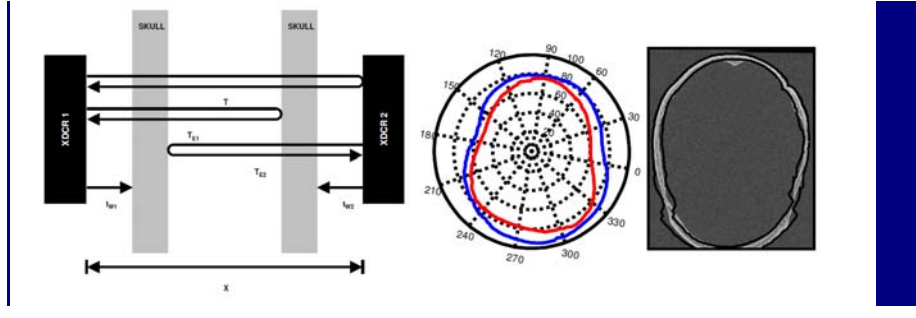
Fig 3 In a **preliminary study on 10 ex vivo formalin-preserved human skulls** transmission and reflection data were acquired around the skull using two 500 kHz transducers on a stepping-motor positioner, giving the data to solve eq (8) (example, center). In the preliminary data, a stepping motor was used to acquire axial slices at 0.5 cm intervals to provide a 3D dataset. However, the preliminary work (Fig. 8) predicts a single axial measurement plane will be sufficient to correct for skull distortion. Discrepancy with CT (right) is a combination of error in the US measurement and also the CT-US registration. Methods will be investigated to minimize this error (Aim 1), however, even with the error present , substantial image improvement results (Fig 2).

Conventional diffraction tomography [9] is based upon sending a series of parallel waves through the region of interest (ROI) over a sequence of rotation angles. A key requirement is that there is negligible contribution to scattering outside the ROI. Utilizing ultrasound's superior ability to be customized, we will design a field whose wavefront is directed into a nearly-parallel beam only within the ROI using our previously-designed numerical projection technique, where the desired field is specified and then rapidly backward-propagated to the imaging transducer. [10], [11] In the present case this will include the effects of the skull bone [12]. Unlike algorithms that only focus ultrasound in a particular location [3], the method is devised to produce arbitrarily-shaped fields within the brain; in the present case a coherent wavefront within the ROI. Subsequent physical transmission of the planned field will then reassemble itself into a coherent wavefront as it propagates through the skull, approximating the planned planar wave once inside the ROI. Unlike prior focusing techniques that required prior CT images, the information necessary to plan this propagation technique will be acquired directly using the ultrasound array (2.2.2). Key novel features of this *first* planning stage include (i) a transmission signal that is optimized to produce a parallel wavefront only within the ROI (ii) with multiple cycles to improve signal strength and allow straightforward mixing of phase shifted shear and longitudinal modes, and (iii) the use of a planned aberration correction to produce a coherent field in the brain. Signal echoes will then be recorded by the array and used in a *second* planning stage. There, the data will be numerically propagated into the brain, again using ultrasound-derived skull data (2.2.2). This modeled propagation will serve to effectively erase the contributions of phase distortion by the bone, providing the approximate signal in the brain, before skull distortion. This corrected field will then be propagated to a *virtual source*, positioned an arbitrary distance from the ROI.

In a departure from standard diffraction tomographic reconstruction, signal inversion will be performed by preselecting a regular grid in the Fourier transform space of the ROI and filling values in this space through an inverse mapping of these locations to points on a the virtual array. This mapping can be contrasted with conventional methods [9], [13-16] that project data *onto* this space, producing a generally incomplete, partially oversampled and irregular dataset requiring interpolation [17], [18]. Rather than pulsed ultrasound, the approach uses a multi-cycle, near-monochromatic, signal to increase the total energy sent to the ROI [19]. The signal advantage will be similar to that of time-extended coded excitation, [20], [21] and would include the addition of a tuned impedance matching network for higher output power to the transducer, if necessary.

At the estimated optimal imaging frequencies (0.75 to 2 MHz), *the thickness resonance of the skull is known to cause periodic frequency dependence on the amplitude of the transmitted signal* [4], [22]. Thus, small changes in skull thickness at different parts of the bone can result in large changes in the optimal transmission frequency (Fig 2). To more uniformly fill the spatial Fourier space of the ROI, we will utilize different imaging frequencies at different positions on the skull. This construction method is possible since the object itself and its transform are ultimately independent of the imaging frequency.
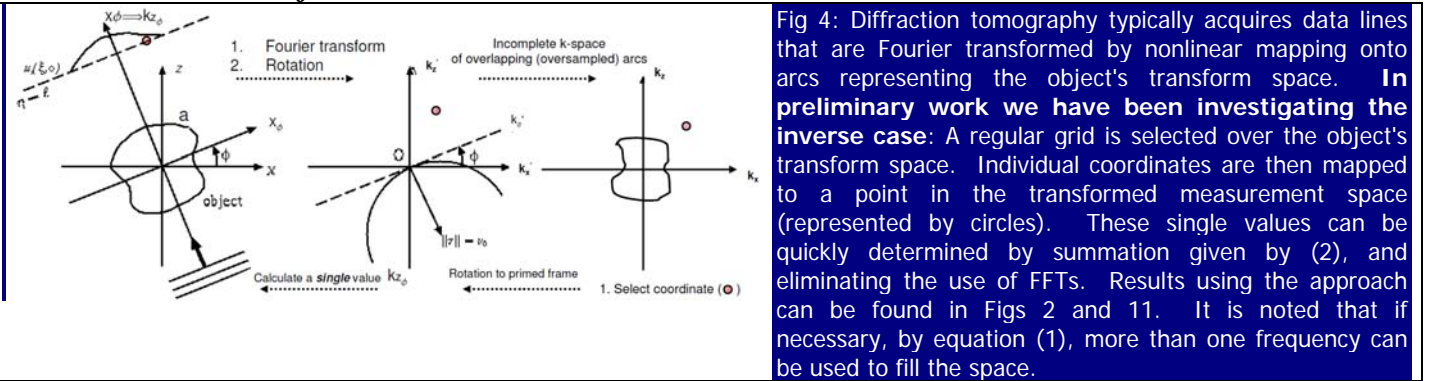
## 2. Skull Characterization

To perform the above imaging, in Year 3 10 ex vivo skulls were used to produce maps of the skull thickness, position and sound speed have been produced, based entirely upon feedback from the imaging array. Because these parameters are designed to be acquired directly from the brain-imaging array, excellent registration between the skull and the imager are achieved. The procedure uses simultaneous acquisition of the transmitted and reflected signals from a small section of the transducer surrounding, or partially surrounding, the head. From time-of-flight measurements, a system of equations is then assembled. The required information includes the time from the transducer to the outer skull surface, the time from the transducer far inner surface. As described in detail ibelow, this information is sufficient to obtain the skull thickness and sound speed under the assumption that the speed is equal on opposite sides of the skull (Fig 3.1). Work over the past year has verified this assumption causes only small errors in the ability to predict phase distortion caused by the bone and is not expected to be a significant factor in the ability to phase-correct the imaging beam. In addition to planning (2.2.1), the data is also be used to form an image of the inner and outer skull layers, providing anatomical landmarks for image orientation (Fig 3.2).

In the first two years of the current project, in combination (separately-funded) clinical investigations, shear-mode windowing has established the ability to access nearly all regions of the brain by using mode conversion in the skull bone [5], [22-24] . This year we considered image reconstruction in the simultaneous presence of both longitudinal and shear modes, as necessarily manifest themselves in allowing signal acquisition over at least 180° for an arbitrarily-selected ROI. The relevant contribution of the signal from each mode of propagation will be determined in the planning stages (2.2.1) as determined by the incident angle available from the skull characterization and imaging (2.2.2).

Considerable value to the planned approach is expected by combining the two modes.

## 3. Selected Method of reconstruction



Fig 4: Diffraction tomography typically acquires data lines that are Fourier transformed by nonlinear mapping onto arcs representing the object's transform space. **In preliminary work we have been investigating the inverse case**: A regular grid is selected over the object's transform space. Individual coordinates are then mapped to a point in the transformed measurement space (represented by circles). These single values can be quickly determined by summation given by (2), and eliminating the use of FFTs. Results using the approach can be found in Figs 2 and 11. It is noted that if necessary, by equation (1), more than one frequency can be used to fill the space.

The first key point of investigation concerns the manner in which the Fourier transform space of the ROI is constructed. We will initially model backscattered signals from a series of quasi-focused planar fields, designed to resemble a quasi-focused wave that is planar only within the ROI (situated, for illustration, on the Cartesian x-z plane, Fig 6). By the standard description of diffraction tomography[9], the backscattered pressure recorded over a line perpendicular to the z-axis, p(x; $z_0$), the relation between the spatial Fourier transform of a received signal and the 2D Fourier transform of the object's scattering coefficient, a(r'), can be expressed as

$$A(\tilde{k}_x', \tilde{k}_z') = A(k_x, \sqrt{k_0^2 - k_x^2} - k_0)\Big|_\theta = \frac{P(k_x;\theta)}{ip_0}\sqrt{k_0^2 - k_x^2}\, e^{iz_0\sqrt{k_0^2 - k_x^2}}, \tag{1}$$

7

where capitols denote transforms, $k_0 = \dfrac{\omega^2}{c_0^{\,2}}$, and $\theta$ represents the rotation angle between the measurement frame and a stationary reference axis.  While various techniques have been described to construct points via rotation of $\theta$ and/or variation of the imaging frequency [17], [25], data are then either interpolated to create a regular grid that can be inverse transformed or nonlinear transform techniques can be utilized, eliminating the need to interpolate.   Conversely, we will directly map coordinates of the object's transform space, $\mathbf{k}' = (k_x^{'}, k_z^{'})$, to coordinates of the projection space, $\mathbf{k} = (k_x, \theta)$, comprised of the transform of the complex acoustic pressure measured along the spatial direction x at a constant value $z_0$ from the origin (Fig 4).  By selecting points in the object's transform space, over-sampling will be avoided while assuring the maximum possible region of the space is filled.  Otherwise stated, interpolation in the measured space is expected to be far less sensitive than interpolation in the object's transform space. This operation is an expected advantage in efficiency, since this operation requires only a single-point calculation of Fourier transformed values,

$$P(k_{xm}, \theta_n) = \frac{1}{\sqrt{2\pi}} \int_{-\infty}^{\infty} p(x, \theta_n) e^{-ik_x x} dx \simeq \frac{\Delta x}{\sqrt{2\pi}} \sum_x p(x, \theta_n) e^{ik_{xm} x}, \tag{2}$$

as opposed to *fast* Fourier transforms, which - despite their namesake - necessarily must calculate all values of k up to the Nyquist frequency for each transform, followed by interpolation to determine the field at the relevant $k_{xm}$.

Noting that A in (1) is written in a rotated frame $\tilde{\mathbf{k}}' = (\tilde{k}_x^{'}, \tilde{k}_z^{'})$ relative to $\mathbf{k}'$,  it must be the case that magnitudes of the position vectors are equal in both frames.  Along with $\tilde{\mathbf{k}}''$'s relation to the projection space, this gives the system of equations

$$\sqrt{\tilde{k}_x^{'2} + \tilde{k}_z^{'2}} - \sqrt{k_x^{'2} + k_z^{'2}} = 0; \; k_x = \tilde{k}_x^{'}; \; \sqrt{k_0^{\,2} - k_x^{\,2}} - k_0 = \tilde{k}_z^{'}. \tag{3}$$

Eliminating $\tilde{\mathbf{k}}$ terms and solving for $k_x$ gives the solutions $\; k_x = \pm \dfrac{\sqrt{(4k_0^{\,2} - k_x^{'2} - k_z^{'2})(k_x^{'2} + k_z^{'2})}}{2k_0}$.  (4)

The angle $\theta$ can be determined using the inner product relation, $\left|\mathbf{k}'\right|\left|\tilde{\mathbf{k}}'\right|\cos\theta = \mathbf{k}' \cdot \tilde{\mathbf{k}}'$. $\tag{5}$

Incorporating this equation into the system of equations presented in (3) and solving for $\theta$ in terms of $k_x^{'}$ and $k_z^{'}$ yields the solutions:

$$\theta = \cos^{-1}\left\{ \pm \frac{k_z^{'}}{2k_0} \pm \frac{\sqrt{k_x^{'2}(4k_0^{\,2} - k_x^{'2} - k_z^{'2})(k_x^{'2} + k_z^{'2})}}{2k_0(k_x^{'2} + k_z^{'2})} \right\}. \tag{6}$$

Our investigation confirmed that it is straightforward to determine relevant solutions by solving for all cases, and then testing for relevant solutions. In the forms given by (4) and (6), reconstructing the object's transform space is then a matter of solving for $(k_x, \theta)$ over the relevant region of space and then determining all values of $P(k_x; \theta)$ that are attainable, noting that $k_x$ and $\theta$ must be real, and that there may be overlap between the solutions.  With the completed array, any advantage of the planned reconstruction will be quantified in terms of the RMS % error between the actual ROI and the reconstructed image as compared to a control forward-based reconstruction.  Differences in the number of computations will also be quantified.

Equation (1) is based upon a spatially-coherent planar source wave traveling parallel to the (rotated) z-axis through the region of interest (ROI) and assumes negligible net contribution from scattering outside the ROI. Improved reconstruction is expected by using a tailored US beam to better approximate these conditions. To realize such a field, a coherent parallel field is numerically planned within the ROI and then back-propagated to

the source (*first planning stage*) [10], [11]. Subsequent physical radiation of the conjugate field pattern [26] over the transducer surface will then approximate the planned ROI, resulting in a field that is optimized only within this region.
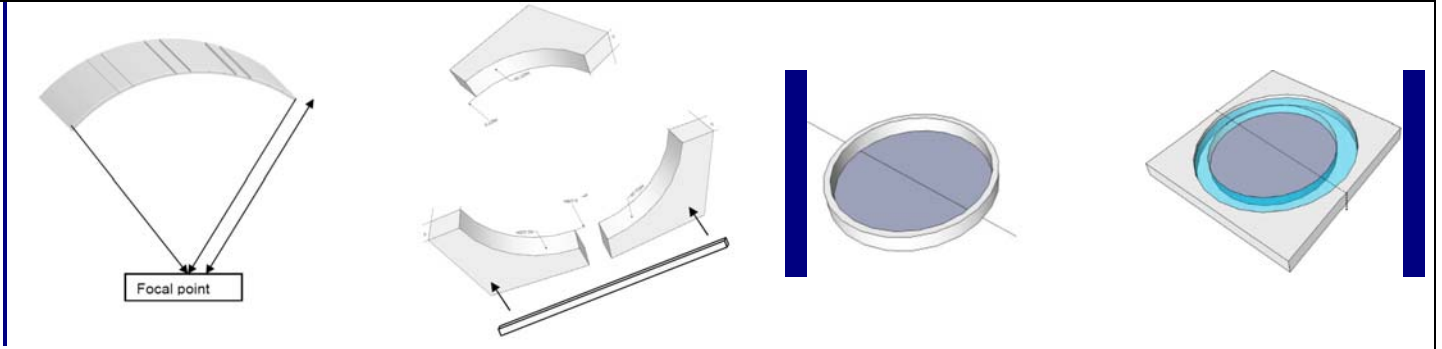


Fig 5: A **preliminary array design study** has centered on 2-4 interlocking modular sections of a backed PZT 1-3 composite for straightforward positioning around the head. Insertable gel-based and water-filled membranes will be considered for optimal coupling. Our ongoing human subject study during brain surgery has confirmed the ability to transmit via shear mode windowing, and to couple US through hair using US gel.

To assure that echoes within the imaging plane reach the receiver, a ring array encompassing the ROI is being constructed (Fig 5). This geometry is also expected to lend itself naturally to the rotations involved in tomography. The received wave will be numerically propagated to a virtual line at $z_0$ in order to perform the image reconstruction (*second planning stage*). To fill the transform space $P(k_x ; \theta)$, the process is repeated over 180 degrees at an optimal angular resolution $\Delta\theta$, which will be determined as part of this study. Specific values of $\theta$ given by (6) require interpolation from the set of measured angles, $\theta_n$, however, by shifting the interpolation to k-space, we have found that interpolation over $\Delta\theta$ produces reduced error compared to the forward case, since the forward mapping produces areas of under- (and over-) sampling, that are avoided in the inverse case.

To summarize, (i) the desired localized planar field in the ROI is planned and numerically and back-propagated to the source. (ii) The space-reversed [27] signal reaching the source is then physically generated using a section of a transducer array, and the resulting echoes received over the transducer. (iii) This signal is numerically propagated to a virtual array located at $z_0$. (iv) The process is repeated to form $p(x,\theta_n)$. (v) Signal inversion is performed by acquiring relevant points from a pre-selected regular grid $(k_x^{'}, k_z^{'})$ in the object's transform space and inverse transformed to produce an object. It is further understood that the skull bone sound-speed and thickness causes frequency dependence on the amplitude of the ultrasound transmitted into and out of the brain (Fig 3). Noting that A in (1) is independent of wave number $k_0$, in the next year we will also investigate the reconstruction of the space using multiple frequencies, as described below (*Spectral transmission*).

## 4. Method of determining skull dimension, and sound speed
Various schemes have demonstrated ultrasound beam correction through the skull, including the use of implanted acoustic sources, or prior CT [3] and MRI as input to phasing models. Noninvasive methods developed by the PI [28], [29] are presently being utilized in clinical trials for brain treatments [30],[31]. In contrast, the approach developed this year is based entirely upon feedback from the ultrasound imaging array. As opposed to focusing to a single point by phase-defining a location, the method is valid for producing arbitrary fields within the brain; the relevant wave in our proposed study being a directed parallel wavefront in the ROI.

The procedure involves the acquisition of both the transmitted and the reflected signals from a small section of an array (Fig 3). This section can be either a single element or several consecutive elements if a stronger and more directed signal is required. The source and transmission receiver is positioned co-axially on opposite sides of the skull and coupled to the head by a standoff material. An impulsive or limited-cycle signal is generated in order to acquire time-of-flight. It is understood that reverberation within the skull bone prevents separation of echoes from the inner and outer skull surfaces at the relatively low frequencies to be used for

penetrating thick bone [19].  Therefore, time-of-flight measurements is obtained using a first-arrival technique from the outer skull, $t_w$, and the far inner skull surface, $T_E$ after traversing the brain.  The transmission time to an opposing array element after crossing through the head, $T$, is also be recorded.  This procedure is repeated from the opposite side, now using the previous transmission receiver as a source, giving times to the outer skull, $t_{w2}$, and far inner skull $T_{E2}$ from the opposite side (Fig 3).

A system of equations is formed with the assumption that the speed of sound in the standoff material and skin, $c_w$, and the brain, $c_B$, are known.  Physiological variation is known to result in significant variation in the longitudinal sound speed between different skulls as well as over the surface of the same skull, [32] so it is not possible to assign a tabulated skull sound speed *a priori* (and the reason impulse-based ultrasound measurement cannot be used to find skull thickness).  To provide a solvable system of equations, the approach first calculates an outline of the outer skull surface by analyzing the values of $t_w$ and $t_{w2}$.  This outer surface allows an approximate angle of incidence to be determined between the skull and the direction of the incident wave.  If an angle of incidence is greater than a given angle (to be determined, but expected to be ~27°) the propagation will be classified as *purely shear* and assigned a tabulated sound speed (1525 m/s).  Otherwise, both modes will be taken into account.   A system of equations will then be assembled.  If at least one side of the skull is traversed via a shear mode, there is, in principle, sufficient information to solve for the thickness and sound speed on both sides of the bone.

However, given multiple modes on both sides of the skull, both sides of the skull is assumed to have the same sound speed, $c_s$, and unknown values for the propagation times within the skull bone $t_s$ and $t_{s2}$, and the skull thicknesses $x_s$ and $x_{s2}$ will be determined from:

$$t_w + t_s + t_B + t_{s2} + t_{w2} = T$$
$$2\,(t_w + t_s + t_B) = T_E$$
$$2\,(t_{w2} + t_{s2} + t_B) = T_{E2}$$
$$c_B t_B + c_w t_w + c_w t_{w2} + x_s + x_{s2} = X \qquad (7)$$
$$c_s t_s = x_s$$
$$c_s t_{s2} = x_{s2},$$

where $X$ is the known distance between the source and transmission transducer. Equation (7) is solvable in terms of the known quantities gives (8):

$$x_s = \frac{(2\,T - T_{E2} - 2t_w)(c_B(2T - T_E - T_{E2}) - 2c_w(t_w + t_{w2}) + 2X)}{8\,T - 2(T_E + T_{E2} + 2(t_w + t_{w2}))}$$

$$x_{s2} = \frac{(2\,T - T_{E2} - 2t_{w2})(c_B(2T - T_E - T_{E2}) - 2c_w(t_w + t_{w2}) + 2X)}{8\,T - 2(T_E + T_{E2} + 2(t_w + t_{w2}))}$$

$$c_s = \frac{c_B(T_E + T_{E2} - 2T) + 2c_w(t_w + t_{w2}) - 2X}{T_E + T_{E2} + 2(t_w + t_{w2}) - 4\,T}.$$

Repeated over 180 degrees, the equations provide the thickness and approximate
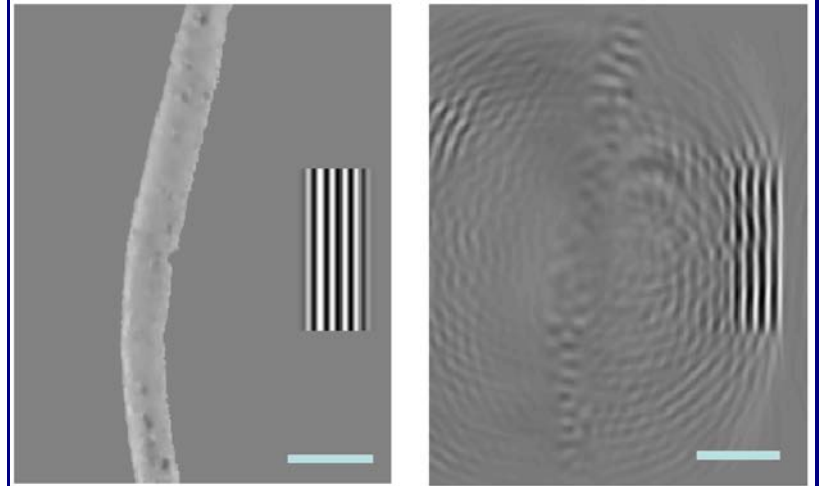


Fig 6: US planning back-propagates in 2D from the desired ROI toward a transducer (left edge of image). In a 3D mock-up of the expected transducer behavior, the conjugated 2D signal reaching the transducer is transmitted by a linear array simulated in 3D, using CT-derived skull data. Results predicted that 2D planning such as that available from ultrasound measurement will provide sufficient beam correction through the skull bone, making near-real-time processing feasible. A resulting single is shown on the right (bar indicates 10 mm).

sound speed in a single plane.  A key finding in this year's work demonstrates that the use of an average sound speed on opposite sides of the skull still allows for substantial phase correction.  The results are formatted into a cross-sectional image of the skull bone, which will be combined with the tomographic image to provide points of reference.   Curve fitting methods are included and assessed for improved accuracy.  Acquired values are also be used in the two planning stages described in more detail below.

For the first metric to evaluate the accuracy of the approach, 10 preserved skulls were affixed to a custom stereotactic reference frame [3] and imaged with CT. The frame allowed us to use a rigid rotation between the ultrasound maps and its corresponding 3D dataset, utilizing the Slicer (3D Slicer V3.6) software package

developed in our affiliated Surgical Planning Laboratory. In practice, each of the measurements were performed twice using our motor-driven rotary table. In the second acquisition, a hydrophone was placed inside the skull to directly determine the time shift caused by the skull. Combined with thickness measurements taken from the CT images, the sound speed was determined and these values were compared with the ultrasound method.

If deemed necessary in the upcoming year, we will introduce more sophisticated methods for evaluating the bone surface, including but not limited to the acquisition of a full B-mode ultrasound image for a more accurate map of the surface, the evaluation of off-axis reflections to determine relevant incident bone angles, and the use of transmission ultrasound to produce a ultrasound tomographic sound speed maps [8].


The initial planning stage entails simulating the desired pressure field within the ROI and back-propagating it to the location of the source transducer using a model that includes the refractive effects of the skull. Once the acoustic pressure is calculated along the array surface, each array element is then be adjusted in amplitude and phase according to the integral pressure value over its surface. Under the approximation that acoustic reciprocity holds, and provided the skull data is sufficiently accurate, the adjusted transmit signal then reassembles itself into an approximately coherent wave as it propagates through the skull and back into the ROI. Studies over the past 12 months outline how a 2D planning model is expected to provide improvement to a 3D problem, suggesting that near-real time processing is feasible (Fig 6). We used a 3D dataset derived from CT images to fully model a minimum of 3 skulls in order to compare differences between 2D and 3D planned fields. If later verification determines that the 2-dimensional information is not sufficient, we will introduce a 3D acquisition of skull dimensions and sound speed and implement a full 3D propagation model for the planning.

In our studies a wave-vector time domain model was utilized, however in the upcoming year we will investigate other model equations and methods of solution for improved accuracy and improved efficiency. The key will be determining the fastest possible method that still yields substantial image improvement. We will compare both fast time-domain and frequency-domain models, in both cases varying the resolution and dimension of the model in order to determine the best tradeoff between accuracy and computational efficiency.

Based on the field modeled over the array surface, the amplitude and phase of relevant elements are adjusted - the past year in simulation, the next year in experiment. Unlike the planning, simulations involve a full 3-dimensional model of the array and skull. Evaluation compared the corrected beam with the ideal wavefront in the ROI with an uncorrected beam; the percent error between the actual and ideal wavefront serving as the metric. These three cases (no skull, corrected, and uncorrected) were used for comparison and evaluation in all stages of the approach.

## Second planning stage
Echoes within the brain are again be subject to skull distortion after being reflected back toward the source, necessitating a second phase correction. This process starts with the distorted signal received by the array. In a numeric process, the conjugate signal is numerically propagated from the array into the brain, reassembling itself in the process as it passes through the skull (Fig 6). Once propagated past the skull, all space outside of the ROI -including the space physically occupied by the skull and brain - isl be modeled as a homogeneous brain-like structure. This virtual space allows the field to be projected to an arbitrary *virtual* array located a distance $z_0$ from the axis of rotation. It is noted that this plane is not necessarily within the confines of the physical brain. This reconstructive second stage will requires a higher resolution model than the first "beam correcting" stage, thus the choice of model was selected independently from the first.

The aforementioned evaluations served to form the base reconstruction algorithm. Once in place, concentration shifted to optimization of the physical parameters of the array. The algorithm was used to evaluate array characteristics (array curvature, element height, element width, curvature along the width, optimal frequency, number of elements, and rotation resolution). To verify frequencies, as well as the overall reconstruction algorithm preliminary experiments were performed using our 128 element linear transskull array (Fig 7) to mimic a section of the full array. In these experiments the skulls were attached to a motor driven rotary table and actively rotated.
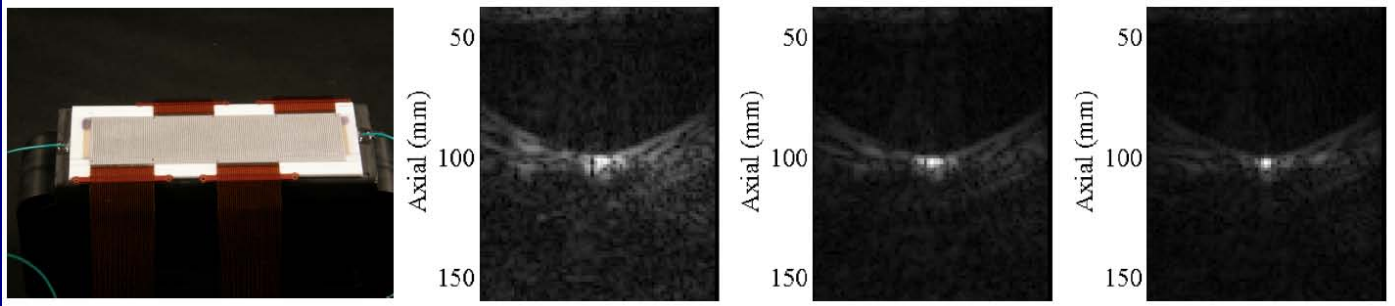
Fig 7. Transcranial measurement using our 128 element transcranial probe (right) provided substantial information leading to the proposed design and method. A study for detecting foreign bodies (small, metallic) in the brain established the ability to image through thick bone (center-left), while also indicating that the images could benefit from phase correction , shown for the transmit pulse (center-right), and both transmit & receive (right).

## Spectral Transmission

Since the thickness resonance of the skull has been shown to cause significant frequency dependence on the amplitude of the ultrasound wave transmitted into the brain [4], we also investigated the idea of utilizing differing imaging frequencies as a function of position. This may prove to be particularly important in reconstruction around the skull, since small changes in skull thickness at different parts of the bone often result in large changes in the optimal transmission frequency (Fig 3). In the procedure, reconstruction points of the object's transform, given by A(k) in (1), are acquired using different temporal frequencies for different k-space coordinates. The validity of assembling this space from different frequency acquisitions lines in the fact that A(k) is ultimately frequency independent. To make the method practical, and recalling that the multi-cycle approach is being used for signal strength, over the next year we will attempt to improve upon image quality using a minimal number of frequencies (2-4). If unsuccessful, we will also attempt to utilize chirped signals which, although stronger in total energy than impulsive signals, are understood to produce weaker signals at a given frequency [19] than the multi-cycle case. However, the advantage of frequency-matching over the skull may prove to outweigh the multi-cycle advantage. In all cases, success will be based on comparing multi-frequency reconstructed images with their single frequency equivalents.

## Final Transducer Design (under construction)

The starting point for our new transducer design was a ring configuration (Fig 5). Modifications to determine the optimal geometry and number of elements were based on preliminary studies, where we estimated the number to be in the range of ~ 500 to 750, with a operational frequency range between ~ 0.650 MHz and 2 MHz. Technical details of complex array design such as crosstalk, mode degeneration, and mode coupling were addressed and assessed during transducer characterization. Our current 128-element linear array was utilized to mock-up the behavior of the ring design to verify performance before final construction. The transducer head, now in construction, will consist of a PZT 1-3 composite material, which will be manufactured and electroded in four sections by a custom manufacturer (Imasonic, Lyon, France) and then wired and assembled in-house.

Fourier analysis of ultrasound pulse-receive sequences was used to determine the response of prototype transducer heads. The mounting of each transducer element and its electrical connection can cause mechanical loading, resulting in amplitude and phase variation between elements. We will investigate these differences by applying the ultrasound field magnitude and phase from the entire transducer in a plane across the beam. A back propagation method was used to virtually propagate these fields back to the transducer face to obtain he acoustic source field for each element. This field was then be used to evaluate array performance and to calibrate individual elements.

We are presently investigating various designs for transducer coupling, with the goals of rapid and straightforward attachment and the ability to couple through the hair, which is predicted based on a relevant study [33]. In past designs we have used water and polymer standoff materials to couple arrays to the head, all of which have been verified in human subjects. We are considering each method, utilizing computer assisted design and mock-ups to determine the most effective and most practical solution.

## Final Driving and Receiving Electronics (under construction)

Signal transmission and reception will be implemented through the modification of one of our existing investigational ultrasound systems. The system currently permits custom output signals to 128 channels and the reception of full RF time traces on 256 channels. The engine generates a bipolar pulse train with individual control of the frequency, phase, amplitude, and pulse length of each channel, allowing an output voltage of up to approximately ±200V over 50Ω across each channel. The design work performed this year expands this system for use with a ring array up to 1024 elements; a number conservatively above the upper estimate of 750 elements expected to be required for the reconstruction.

A design for this switching has been tested for feasibility and budget estimates (Fig 8). Two key design aspects have substantially simplify the network. First, we found from preliminary ultrasound field measurement that that a maximum of 25% of the array will be required for any given acquisition. Second, the existing system's capability of software controlling individual elements will reduce the switching demand to only four dedicated array elements per channel and switching of only a single channel per rotation. The modification thus involves the addition of a computer-controlled relay network that will switch between quadrants of the ring array. Initially, a prototype board was constructed for troubleshooting. This board will be modified in the upcoming months to create a working design that is tested and verified with the ultrasound system. The final, multi-layer PCB design will be professionally manufactured and the circuit completed in-house.
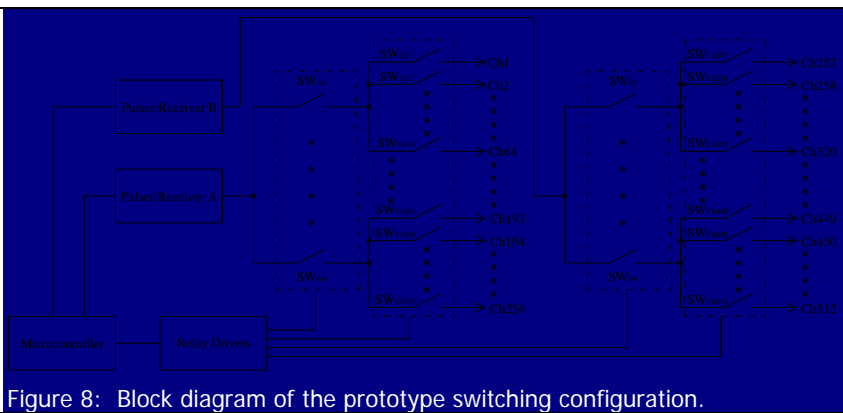


Figure 8: Block diagram of the prototype switching configuration.

## Software

Software is actively being developed in three separate modules, followed by integration into a single software package. The modules represent the three major computing tasks required for the project: control, algorithm implementation, and user interface. In the upcoming year, control software will be written to provide input signals to individual elements of the driving system, record time traces from each element, and coordinate between the ultrasound engine and the hardware switching. Specific tasks for the module will be to operate the array in a time-of-flight transmission and echo mode to provide data on the skull geometry and properties, transmission of the planned waveform, reception of echoes, and interfacing with the algorithm software between each stage. The algorithm software determines skull parameters, perform planning, and implement the tomographic reconstruction based on data passed from the control software. Concentration is on rapid implementation, making use of parallelizable code. While near-real time operation was not included in investigative work over the past year, the present goal will be to perform the imaging over a sequence of approximately 30s of CPU time per channel, which parallelized on a 16 CPU PC would allow an image to be formed in a period of approximately 5 minutes, with speed optimization to be planned following positive result from the present study. Display and interface software was tested allowing user to control the mode of imaging, the image parameters and provide various image output modes though a graphic user interface. Mirroring past projects, [34-36] the features have been largely selected through radiologist comments and feedback.

## Experiments with ex vivo Tissues

Experiments were performed with our collection of preserved *ex vivo* human calvaria samples (N = 22) and brain-mimicking dual MRI-ultrasound phantoms to ascertain specific details of the backscatter tomography. Our existing phantoms (N = 26) were developed to mimic the tabulated acoustic and MR properties of the gross brain anatomy and separately: fluid and solid cysts, foreign bodies, brain deformation, hemorrhaging, and hydrocephalus. Additionally, we are in the process of constructing an ultrasound/MRI/CT full anatomical normal brain phantom in cooperation with, and based on the work of the McConnell Brain Imaging Centre, Montreal Neurological Institute, McGill University, Montreal, Canada [37]. Completion of this phantom is expected in Mid 2011, and is expected to substantially aid the proposed project in pre-clinical assessment of the ability to image normal brain features. In the evaluation procedure phantoms are be placed inside a calvarium and then affixed to a custom stereotactic reference frame [3] containing MR-fiducial markers before

13

acquiring MR-images. The stereotactic frames allow for co-registration between the ultrasound transducer and the MR-images, and provide a means of quantitatively comparing image frames. For ultrasound testing, the entire transducer is submerged in a underwater test tank. Each phantom's reference frame is attached to a 3-dimentional positioning system, whose coordinates will be calibrated with the transducer array. We then utilize co-registration software (3D Slicer V3.6) to compare images. The optimal ROI area were determined to be approximately an $20cm^2$ to $30cm^2$ in the brain when imaged through the skull, which can then be repeated over a regular grid in order to cover an entire planar section through the brain.

In the upcoming year the images will be assessed for signal level and distortion as a function of relative position within the brain and as a function of the relative alignment of the transducer. Other factors affecting accuracy and signal strength , including relative position of the imaging plane, the and the use of longitudinal versus shear modes of ultrasound propagation in the skull bone will also be determined, in each case using co-registered MRI to benchmark performance.
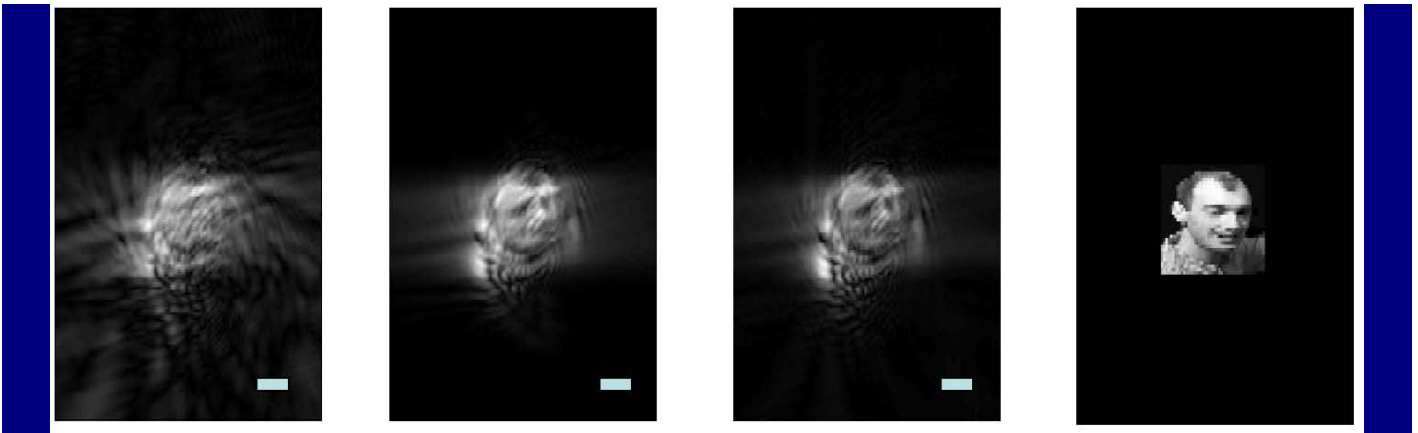


Fig 9. A **Preliminary study on resolution potential** generated numeric skulls with random thickness and sound speed and simulating a photo 'tumor' (used to illustrate detail). Shown here is a 1.25 MHz reconstruction (bar = 10 mm). Reconstructions without treatment planning (left) and including planning (center-left) are compared to tomography without the skull layer (center-right). The original image is provided for reference (left). Further improvement is expected by using multi-freq reconstruction to fill the transform space, improve transmission, and reduce artifacts. Manipulation of frequency (not shown) also provides a means of controlling the balance between resolution and signal strength.

# KEY RESEARCH ACCOMPLISHMENTS

As highlighted throughout the report, substantial information was gained from the initial array design, resulting in an improved and unique approach for the final applicator that will be capable of operating as a full (ring-shaped) brain imager, or in part (1/4 array) as a foreign body detector. Year 3 represents extensive progress toward producing a portable ultrasound device that, if successfully validated over the period of the 1-year no cost extension to the grant, will offer unsurpassed brain imaging quality for an ultrasound device, portable or otherwise.

# REPORTABLE OUTCOMES (Past 12 months)

C. Mearl and G.T. Clement, "128 Element Ultrasound Array for Transcranial Imaging," IEEE International Ultrasonics Symposium Proceedings, 2010 IN PRESS

G.T. Clement, "Planar projection in absorbing media possessing an arbitrary dispersion relation" Acoustical Science and Technology. 2010; 31(6): 379-386.

# CONCLUSION

We have demonstrated over the past 12 months that - through a combination of new beamforming, planning, and reconstruction techniques - a more effective means for US imaging through the skull is possible (Figs 2, 4,11). In the upcoming year the completed device and method will be extensively verified, and various modes of operation will be studied. The completed study will provide a device ready for clinical testing, thus providing a platform for investigation in a wide range of settings and conditions.

# REFERENCES

[1]    A. H. Andersen, "A ray tracing approach to restoration and resolution enhancement in experimental ultrasound tomography," *Ultrasonic Imaging*, vol. 12, no. 4, pp. 268-291, Oct. 1990.

[2]    F. Simonetti, L. Huang, N. Duric, and P. Littrup, "Diffraction and coherence in breast ultrasound tomography: a study with a toroidal array," *Medical Physics*, vol. 36, no. 7, pp. 2955-2965, Jul. 2009.

[3]    G. T. Clement and K. Hynynen, "A non-invasive method for focusing ultrasound through the human skull," *Physics in Medicine and Biology*, vol. 47, no. 8, pp. 1219-36, Apr. 2002.

[4]    J. Aarnio, G. T. Clement, and K. Hynynen, "A new ultrasound method for determining the acoustic phase shifts caused by the skull bone," *Ultrasound in Medicine & Biology*, vol. 31, no. 6, pp. 771-80, Jun. 2005.

[5]    G. T. Clement, P. J. White, and K. Hynynen, "Enhanced ultrasound transmission through the human skull using shear mode conversion," *The Journal of the Acoustical Society of America*, vol. 115, no. 3, pp. 1356-64, Mar. 2004.

[6]    S. W. Smith, O. T. von Ramm, J. A. Kisslo, and F. L. Thurstone, "Real time ultrasound tomography of the adult brain," *Stroke; a Journal of Cerebral Circulation*, vol. 9, no. 2, pp. 117-122, Apr. 1978.

[7]    D. Phillips, S. W. Smith, O. von Ramm, and F. Thurstone, "A phase compensation technique for B-mode echoencephalography," *Ultrasound in Medicine*, vol. 1, pp. 395-404, 1975.

[8]    G. T. Clement and K. Hynynen, "Ultrasound phase-contrast transmission imaging of localized thermal variation and the identification of fat/tissue boundaries," *Physics in Medicine and Biology*, vol. 50, no. 7, pp. 1585-600, Apr. 2005.

[9]    A. C. Kak and M. Slaney, *Principles of Computerized Tomographic Imaging*. Society for Industrial Mathematics, 2001.

[10]  G. T. Clement and K. Hynynen, "Field characterization of therapeutic ultrasound phased arrays through forward and backward planar projection," *The Journal of the Acoustical Society of America*, vol. 108, no. 1, pp. 441-446, Jul. 2000.

[11]  G. T. Clement, R. Liu, S. V. Letcher, and P. R. Stepanishen, "Temporal backward planar projection of acoustic transients," *The Journal of the Acoustical Society of America*, vol. 103, no. 4, pp. 1723-1726, Apr. 1998.

[12]  P. White, B. Andre, N. McDannold, and G. Clement, "A pre-treatment planning strategy for high-intensity focused ultrasound (HIFU) treatments," in *Ultrasonics Symposium, 2008. IUS 2008. IEEE*, pp. 2056-2058,

2008.

[13] R. K. Mueller, "Diffraction tomography I: The wave-equation," *Ultrasonic Imaging*, vol. 2, no. 3, pp. 213-222, Jul. 1980.

[14] B. A. Roberts and A. C. Kak, "Reflection mode diffraction tomography," *Ultrasonic Imaging*, vol. 7, no. 4, pp. 300-320, Oct. 1985.

[15] B. S. Robinson and J. F. Greenleaf, "The scattering of ultrasound by cylinders: implications for diffraction tomography," *The Journal of the Acoustical Society of America*, vol. 80, no. 1, pp. 40-49, Jul. 1986.

[16] S. Mensah and R. Ferriere, "Diffraction tomography: a geometrical distortion free procedure," *Ultrasonics*, vol. 42, no. 1, pp. 677-682, Apr. 2004.

[17] M. M. Bronstein, A. M. Bronstein, M. Zibulevsky, and H. Azhari, "Reconstruction in diffraction ultrasound tomography using nonuniform FFT," *IEEE Transactions on Medical Imaging*, vol. 21, no. 11, pp. 1395-1401, Nov. 2002.

[18] D. Rouseff, L. Tsang, and R. P. Porter, "Diffraction tomography by a method of image projections," *Ultrasonic Imaging*, vol. 10, no. 3, pp. 204-219, Jul. 1988.

[19] G. T. Clement, "Spectral image reconstruction for transcranial ultrasound measurement," *Physics in Medicine and Biology*, vol. 50, no. 23, pp. 5557-72, Dec. 2005.

[20] M. O'Donnell, "Coded excitation system for improving the penetration of real-time phased-array imaging systems," *IEEE Transactions on Ultrasonics, Ferroelectrics, and Frequency Control*, vol. 39, no. 3, pp. 341-351, 1992.

[21] T. X. Misaridis et al., "Potential of coded excitation in medical ultrasound imaging," *Ultrasonics*, vol. 38, no. 1, pp. 183-189, Mar. 2000.

[22] P. J. White, G. T. Clement, and K. Hynynen, "Local frequency dependence in transcranial ultrasound transmission," *Physics in Medicine and Biology*, vol. 51, no. 9, pp. 2293-305, May. 2006.

[23] P. J. White, G. T. Clement, and K. Hynynen, "Longitudinal and shear mode ultrasound propagation in human skull bone," *Ultrasound in Medicine & Biology*, vol. 32, no. 7, pp. 1085-96, Jul. 2006.

[24] P. J. White, K. Hynynen, and G. Clement, "Longitudinal and Shear Mode Ultrasound Propagation in Human Skull Bone," in *AIP Conference Proceedings*, pp. 251-255, 2006.

[25] S. Pourjavid and O. Tretiak, "Ultrasound imaging through time-domain diffraction tomography," *IEEE Transactions on Ultrasonics, Ferroelectrics, and Frequency Control*, vol. 38, no. 1, pp. 74-85, 1991.

[26] N. N. Bojarski, "Generalized reaction principles and reciprocity theorems for the wave equations, and the relationship between the time-advanced and time-retarded fields," *The Journal of the Acoustical Society of America*, vol. 74, no. 1, pp. 281-285, Jul. 1983.

[27] G. T. Clement, "Spatial backward planar projection in absorbing media possessing an arbitrary dispersion relation," *Acoustical Science and Technology*, vol. 31, no. 6, pp. 379-386, 2010.

[28] K. Hynynen and G. T. Clement, "United States Patent: 6770031 - Ultrasound therapy," U.S. Patent 677003103-Aug-2004.

[29] K. Hynynen and G. T. Clement, "United States Patent: 7344509 - Shear mode therapeutic ultrasound," U.S. Patent 734450918-Mar-2008.

[30] E. Martin, D. Jeanmonod, A. Morel, E. Zadicario, and B. Werner, "High-intensity focused ultrasound for noninvasive functional neurosurgery," *Annals of Neurology*, vol. 66, no. 6, pp. 858-861, Dec. 2009.

[31] N. McDannold, G. T. Clement, P. Black, F. Jolesz, and K. Hynynen, "Transcranial magnetic resonance imaging- guided focused ultrasound surgery of brain tumors: initial findings in 3 patients," *Neurosurgery*, vol. 66, no. 2, pp. 323-332; discussion 332, Feb. 2010.

[32] G. T. Clement and K. Hynynen, "Correlation of ultrasound phase with physical skull properties," *Ultrasound in Medicine & Biology*, vol. 28, no. 5, pp. 617-24, May. 2002.

[33] S. B. Raymond and K. Hynynen, "Acoustic transmission losses and field alterations due to human scalp hair," *IEEE Transactions on Ultrasonics, Ferroelectrics, and Frequency Control*, vol. 52, no. 8, pp. 1415-1419, Aug. 2005.

[34] S. C. Tang, G. T. Clement, and K. Hynynen, "A computer-controlled ultrasound pulser-receiver system for transskull fluid detection using a shear wave transmission technique," *IEEE Transactions on Ultrasonics, Ferroelectrics, and Frequency Control*, vol. 54, no. 9, pp. 1772-83, Sep. 2007.

[35] P. J. White, S. Whalen, S. C. Tang, G. T. Clement, F. Jolesz, and A. J. Golby, "An intraoperative brain shift monitor using shear mode transcranial ultrasound: preliminary results," *Journal of Ultrasound in Medicine: Official Journal of the American Institute of Ultrasound in Medicine*, vol. 28, no. 2, pp. 191-203, Feb. 2009.

[36] J. S. Thierman, G. T. Clement, L. A. Kalish, P. L. O'Kane, F. Frauscher, and H. J. Paltiel, "Automated sonographic evaluation of testicular perfusion," *Physics in Medicine and Biology*, vol. 51, no. 14, pp. 3419-32, Jul. 2006.

[37] S. J. Chen, P. Hellier, J. Gauvrit, M. Marchal, X. Morandi, and D. L. Collins, "An anthropomorphic polyvinyl alcohol triple-modality brain phantom based on Colin27," *Medical Image Computing and Computer-Assisted Intervention: MICCAI ... International Conference on Medical Image Computing and Computer-Assisted Intervention*, vol. 13, no. 2, pp. 92-100, 2010.